

RESEARCH

Open Access



# Developing constitutive model parameters via a multi-scale approach

B. S. Anglin<sup>1\*</sup>, B. T. Gockel<sup>2,3</sup> and A. D. Rollett<sup>3</sup>

\* Correspondence:

banglin@alumni.cmu.edu

<sup>1</sup>Materials Response and Design  
Branch, US Army Research  
Laboratory, 4600 Deer Creek Loop,  
Aberdeen Proving Ground, MD  
21005, USA

Full list of author information is  
available at the end of the article

## Abstract

Computing the mechanical response of materials requires accurate constitutive descriptions, especially their plastic behavior. Furthermore, the ability of a model to be used as a predictive, rather than a descriptive, tool motivates the development of physically based constitutive models. This work investigates combining a homogenized viscoplastic self-consistent (VPSC) approach to reduce the development time for a high-resolution viscoplastic model based on the fast Fourier transform (FFT). An optimization scheme based on a least-squares algorithm is presented. The constitutive responses of copper, interstitial-free steel, and pearlite are investigated, and the model parameters are presented. Optimized parameters from the low-fidelity model provide close agreement (<2 MPa, ~1 % error) with stress-strain data at low strains (<10 %) in the high-fidelity FFT model. Simple adjustments to constitutive law parameters bring the FFT stress-strain curve in alignment with experimental data at strains greater than 10 %. A two-phase constitutive law is developed for a pearlitic steel using a single stress-strain curve, supplemented by data for the constituent phases. Sources of error and methods of using material information are discussed that lead to optimal estimates of initial parameter values.

**Keywords:** Optimization, Constitutive law, Pearlite, Viscoplastic, Multi-scale

## Background

The usefulness and predictive value of a material model is dependent on two factors: the range over which the description of the mechanisms and physics included in the model are applicable and the parameters used to accurately tune a model to measured results. The determination of the latter has been an active area of research for many years [1]. This central objective is foremost in nearly all modeling applications, which transcends a multitude of engineering fields because it can be applied to problems all the way from fundamental material research up to product design. While many fields can benefit from such a model, the acceptable computational time varies based on the application and intended end user. While researchers may be able to wait weeks for a solution, product designers may be willing to wait only a matter of seconds. From continuum power-law plasticity models to highly detailed crystal plasticity, full-detailed physically based models and short computation times are often mutually exclusive.

This study explores a hardening model embedded within two crystal plasticity frameworks: a homogenized viscoplastic self-consistent (VPSC) algorithm [2] and a full-field viscoplastic model based on the fast Fourier transform (VP-FFT) [3]. Both frameworks

utilize the same core set of viscoplastic crystal plasticity descriptions, relating local stress tensors to local shear rate tensors, and microstructure texture information to predict the constitutive response and texture development of the material microstructure. However, these two frameworks differ in the level of detail utilized and computation time required for simulation. The VPSC code is a serial code that can be run in seconds on a personal laptop where the effect of each grain's environment is homogenized, while the VP-FFT microstructure is discretized to generate full-field solutions and is a parallelized code that was formulated for use on a supercomputer requiring minutes to hours to compute similar microstructures.

Constitutive laws that relate local stress tensor and crystal geometry to the local strain rate tensor control the stress-strain responses of these methods. A hardening law, contained within the constitutive law, prescribes the local stress at which shear will occur on a given slip system and evolves with accumulated strain. In order to predict the stress response of a material, the appropriate parameters for the hardening model must be developed because no theory exists to predict them a priori [4]. These parameters can be determined through manual iterative educated guessing or purely mathematical optimization. Even for a simple material response, this can be excessively time consuming. Such a method coupled with the VP-FFT code could require weeks of trial and error.

Adjusting parameters in equations, a.k.a. curve fitting, is a ubiquitous approach for development of constitutive laws in all materials, ranging from polymers [5–7] to metals [8–15] to nanocomposites [16] to geological materials [17] and even to construction materials [18]. It is used with simple [13] to complex, multiphase models [8] under loading conditions such as uniaxial tension [10], creep, and fatigue [19]. Decreasing simulation computation time during curve fitting is advantageous for quicker constitutive law development. Previous studies typically achieved this by first fitting physical parameters to analytical curves and using single element finite element (FEM) simulations [12], while others have used multi-step optimization approaches [8]. The novelty of the approach used here is a separate simulation tool in which only grain averages are computed (i.e., VPSC) compared to the full-field VP-FFT to reduce curve-fitting time. It is shown that VPSC provides an adequate first guess for the constitutive law used in the full-field VP-FFT with minimal adjustments required. We offer this work in the spirit of the Materials Genome Initiative, namely, as a method for encoding data on the mechanical behavior of materials in a form that can be used for a broad range of scientific and engineering purposes.

The remainder of this manuscript is laid out as follows. The “Background” section consists of the background and theory of the computational models utilized. The “Methods” section contains the optimization scheme in MATLAB utilized to find best-fit parameters within VPSC and a discussion of the materials investigated within this study. In the “Results and discussion” section, the results of the optimizations and how the parameters fare in the VP-FFT predictions of viscoplastic response are presented and discussed for the three materials considered. A comparison of the texture evolution between VPSC and VP-FFT is also presented. Additionally, the dependence of constitutive law parameters on the VP-FFT domain size is discussed. Finally, conclusions are provided in the “Conclusions” section.

### VPSC

The VPSC computer code used in this study was developed at Los Alamos National Laboratory with applications to a range of materials such as copper, titanium, and steels [20–22] and complex loading histories [23].

#### Local constitutive behavior

Modeling viscoplastic material deformation is largely dependent on local orientation and available slip systems for each orientation and loading condition. A non-linear rate-sensitive constitutive model, Eq. 1, dictates the local material behavior by relating the stress state, orientation, and slip system activities to the local tensor strain rate [24], where the sum is over all active slip systems with index  $s$ .

$$\dot{\epsilon}_{ij}(\mathbf{x}) = \sum_s m_{ij}^s \dot{\gamma}^s(\mathbf{x}) = \dot{\gamma}_o \sum_s m_{ij}^s \left( \frac{m_{kl}^s \sigma_{kl}(\mathbf{x})}{\hat{\tau}_s} \right)^n \quad (1)$$

The deviatoric stress and strain rate tensors  $\sigma_{kl}(\mathbf{x})$  and  $\dot{\epsilon}_{ij}(\mathbf{x})$ , respectively, are related by the symmetric Schmid tensor,  $m_{ij}^s$ , which resolves the local stress on to slip system  $s$  by the combination of the slip plane normal,  $\mathbf{n}^s$ , and (normalized) Burgers vector,  $\mathbf{b}^s$ , of the slip system, where  $m_{ij}^s = \frac{1}{2} (n_i^s b_j^s + n_j^s m_i^s)$ . The threshold stress value for each slip system is given by  $\hat{\tau}_s$  and is computed at each strain level by a hardening law. The local shear rate on slip system  $s$ ,  $\dot{\gamma}^s(\mathbf{x})$ , is computed with Eq. 2.

$$\dot{\gamma}^s(\mathbf{x}) = \dot{\gamma}_o \left( \frac{m_{kl}^s \sigma_{kl}(\mathbf{x})}{\hat{\tau}_s} \right)^n \quad (2)$$

$\dot{\gamma}_o$  is a normalization factor, typically assigned a value of 1, and  $n$  is the rate sensitivity exponent, typically assigned a value of 10. This constitutive equation provides a meso-scale description of the viscoplastic deformation response of a polycrystalline material aggregate.

The VPSC algorithm makes use of the Eshelby [25, 26] solution approach by treating each “grain” (i.e., crystal orientation) as an ellipsoidal inclusion contained within a homogenous medium. The homogenous medium in this case is the average response of the grains. The input list of grains (texture information) is a weighted list of orientations (parameterized as the Euler angles), and therefore, no spatial information is required or used [2]. Self-consistency is enforced through ensuring that the average strain rate of the sum of the grains is consistent with the macroscopically applied strain rate. Thus, in the VPSC model, the stresses are calculated across an average based on the collection of grains and can be fully anisotropic. It allows for each individual grain to have a local strain rate that differs from the ensemble average value, thereby weakening the boundary conditions of the Taylor model, which enforces uniform strain rate over all grains. The extent of the local variations depends on the interaction model adopted, which in this case was the affine model.

#### Hardening model

Because VPSC predicts the stress-strain evolution over a prescribed strain path, a hardening model must be utilized and is implemented as the critical resolved shear stress term,  $\tau_0^s$  in Eq. 1. The hardening model predicts the evolution of stress due to

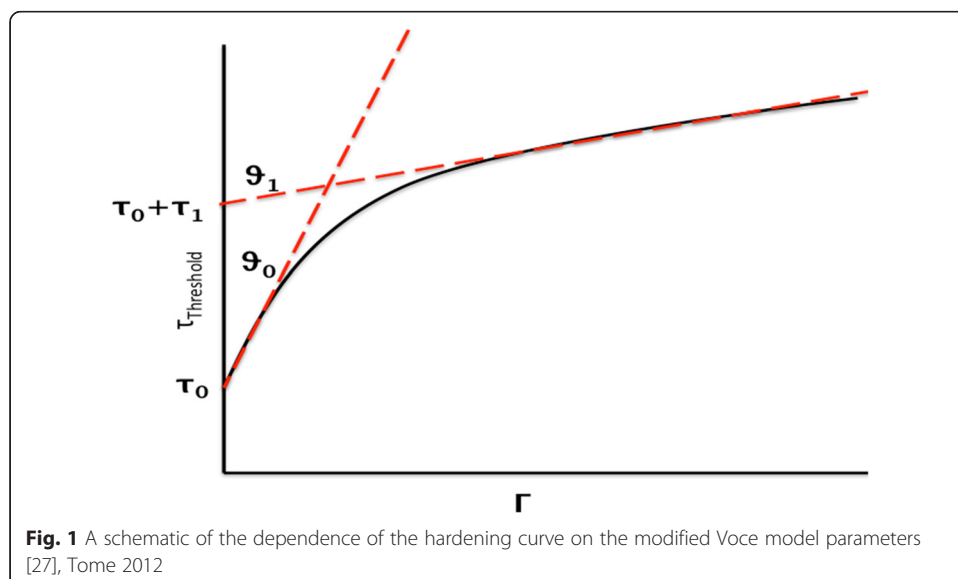
accumulated shear strain in each grain [27]. An extended version of the original Voce hardening model [28], a function of the accumulated shear strain on each slip system  $\Gamma$ , was used for this application, as in Eq. 3.

$$\hat{\tau}_s = \tau_0^s + (\tau_1^s + \theta_1^s \Gamma) \left( 1 - \exp \left[ -\Gamma \left| \frac{\theta_0^s}{\tau_1^s} \right| \right] \right) \quad (3)$$

The parameters within the modified Voce model are  $\tau_0$ , which is analogous to the initial critical resolved shear stress (CRSS), and  $\tau_1$ , which captures the magnitude of the steady-state hardening stress, and  $\theta_0$  and  $\theta_1$  model the initial and steady-state slope of the hardening (or softening) behavior, respectively. Based on this, estimated values of the parameters can be determined from a macroscopic stress-strain plot by utilizing relationships from a microscopic shear stress-strain plot, shown in Fig. 1. To bridge the two disparate length scales, the Taylor factor can be utilized [29]. One set of parameters is required for each slip mode (i.e., combination of slip plane families and family of directions). While the set of parameters need not be unique for separate modes, it can be changed in accord with more detailed knowledge of the CRSS for a given slip mode. In fact, in anisotropic materials such as hexagonal metals, anisotropy and texture development is used to calibrate such values [30].

**VP-FFT**

The viscoplastic FFT method is built upon the same theorems, principles, and constitutive law as VPSC. While VPSC utilizes a homogenization (i.e., Eshelby) scheme to compute the grain average stress and strain values, the VP-FFT method uses high-resolution spatial and Fourier grids over which an FFT is performed to compute the full-field solution. Therefore, spatial resolution of the microstructure is achieved. The discretized spatial grid in VP-FFT resolves each grain at whatever resolution is deemed necessary, providing orders of magnitude more degrees of freedom and spatially resolved grain-level detail. Microstructural input for the VP-FFT is a crystal orientation



for each discretized point within the domain, including a phase identifier. Phase identification is used to assign slip modes and the associated hardening parameters specific to the phase.

The VP-FFT is akin to FEM-based crystal plasticity methods, but as mentioned in the preceding paragraph, the grain structure of a material in a VP-FFT simulation is represented by a regularly discretized grid (i.e., cuboidal “elements”) while in FEM simulations arbitrarily shaped hexahedral elements are admissible. Full-field solutions satisfying local equilibrium and compatibility constraints are achieved in the VP-FFT by use of a Green’s method approach. Use of an FFT to compute the convolution integral required for the Green’s method reduces computation time and improves computational efficiency over most FEM simulations. This reduced computation time and improved efficiency, providing an efficient means for studying microstructures that require high-resolution representation, such as pearlite. Full details of the mathematics of the VP-FFT method can be found in Lebensohn [3].

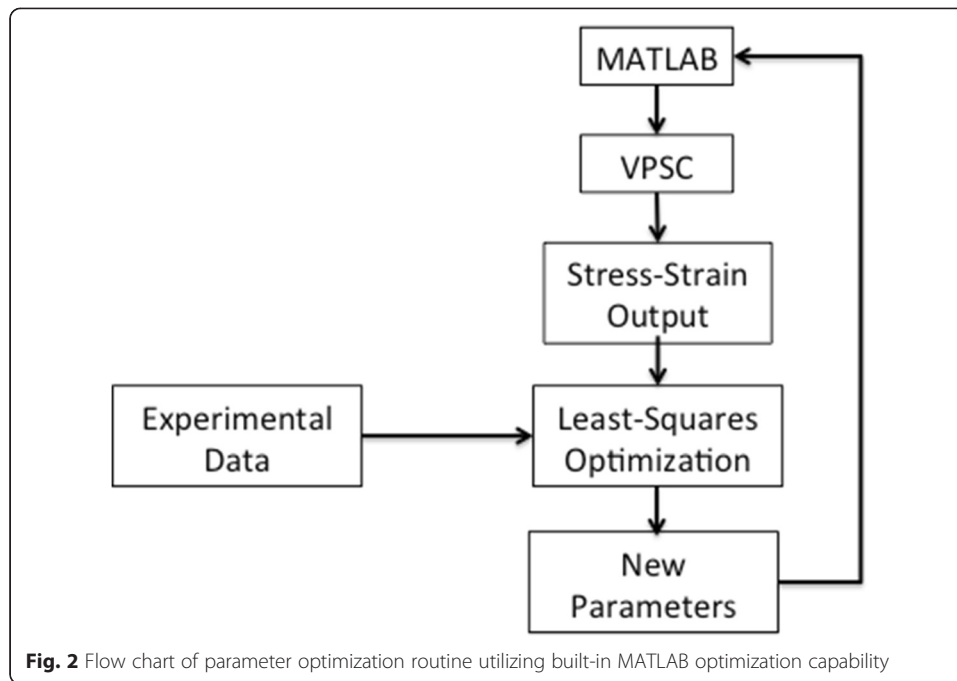
With the addition of microstructural detail comes an additional computation cost. Similar methods for computing the viscoplastic response of material microstructures exist in the FEM framework; however, the primary advantage of this spectral method is efficiency and reduced computation time, especially FEM simulations of comparable sizes. The FFT method has been parallelized with the FFTW library providing additional reductions in computation times [31, 32]. These reduced computation times, regardless of the number of processors used, will not overtake the speed provided by the homogenization approach in VPSC.

## Methods

### Optimization method

In order to more efficiently fit the Voce hardening model to an experimental stress-strain curve within the construct of the VP-FFT code, the similarity of the VPSC code is exploited by pairing it with a MATLAB-based optimization routine. By taking advantage of VPSC’s inherent computation speed, a better informed initial model parameter guess can be made for the more computationally expensive VP-FFT simulations, thus reducing the number of expensive simulations required to fit an experimental curve. The method used was the least-squares optimization routine contained within MATLAB’s optimization toolbox. The least-squares routine attempts to minimize the sum of the square of the difference between the experimental and predicted stress value at each strain step. A schematic of the method that was implemented is shown in Fig. 2, and additional details can be found in Appendix I.

While the extended Voce equation only requires four parameters to be optimized, the least-squares curve-fit algorithm does not guarantee a unique solution. In fact, the initial guess can influence the final solution if the function contains local minima. Thus, one must check the optimized solution to ensure that it provides a reasonable description of the stress-strain behavior, as well as satisfying the least-squares algorithm. For example, the error returned by the fitting procedure may be small, but the shape of the fitted function might suggest that extrapolation beyond the fitted range would lead to large errors.



### Materials investigated

The optimization of the Voce parameters using the VPSC code and the subsequent application to the VP-FFT code is tested with three material systems: 99.9999 % pure copper, interstitial-free (IF) steel, and pearlite. Copper is selected as a fitting exercise as a proof-of-concept of the optimization scheme presented here. The  $\tau_0$ , along with the average Taylor factor, obtained for the IF steel will be used to scale the  $\tau_0$  value for pearlitic ferrite due to the lamellar spacing.

### Copper

In a previous study [33], a well-annealed 99.9999 % pure copper specimen was prepared with a gauge section for a high-energy X-ray diffraction microscopy (HEDM) measurement under progressive tensile loading to evaluate the microstructural changes due to plastic deformation [34]. A roughly  $300 \times 300 \times 100$  voxelized domain of orientation information was measured and subsequently processed to provide phase and grain identifications for use in the VP-FFT simulation containing about 7000 grains. A weak crystallographic texture was present in the initial measurement. Therefore, deviations from sampling the orientations are considered small. A  $64 \times 64 \times 64$  extraction from the strictly solid measured domain containing 213 grains is used in this study. VPSC simulation input is a sampled list of 500 crystal orientations from the original volume, weighted evenly. The resulting stress-strain curve data generated during the previous study, out to 20 % strain, is used as the target for this material. Both computational approaches used 200 time steps with a 0.1 % strain step size.

### IF steel

IF steel contains low amounts of carbon and other alloying elements, resulting in a relatively simple polycrystalline microstructure. A synthetic voxelized microstructure for use in VP-FFT was generated using DREAM3D [35] with a log-normal grain size

distribution and random orientation distribution in accord with the cubic crystal symmetry. The microstructure contained 465 grains and was on a  $256 \times 256 \times 256$  voxelized domain. The resulting list of the 465 crystal orientations was used as input to VPSC. As part of the synthetic structure generation, a crystal orientation was assigned to each grain. The orientation list for VPSC input assumed equal weight of all grains. Thus, the VPSC and VP-FFT starting orientation distributions were equivalent save small variations due to the log-normal size distribution in the VP-FFT input microstructure. The stress-strain data used as the target for parameter development was a tensile test taken to 18.3 % strain [36]. VPSC and VP-FFT used 183 and 18 time steps with 0.1 and 1 % step sizes, respectively.

### Pearlite

Pearlite is a lamellar structure of bcc  $\alpha$ -Fe and orthorhombic cementite. Monolithic cementite is a brittle material, but in pearlite the lamellar structure stabilizes the cementite allowing it to deform plastically [37, 38]. Because of the computational methods used in this study, it is assumed that cementite deforms by slip.

Synthetic pearlite structures were constructed in a  $243 \times 243 \times 243$  domain containing 31 parent ferrite grains with random orientations. Inside these ferrite grains, 226 cementite lamellae (12.8 % by volume) were placed with planar interfaces parallel to the habit plane described by the Bagaryatsky orientation relationship (i.e.,  $\{112\}$ ) between the two phases [39]. Cementite lamellae are placed with a 16-voxel separation and 2-voxel thickness, which represent the thicknesses of the ferrite and cementite layers, respectively. The synthetic reconstruction is shown in Fig. 3. The stress-strain curve used for parameter fitting was from a wire-drawing experiment of commercially pure eutectoid pearlitic steel, 0.85 wt.% C, drawn to 150 % true strain [40, 41]. VPSC and VP-FFT simulations were carried out to strains of 70 and 61 % with step sizes of 0.1 and 1 %, respectively.

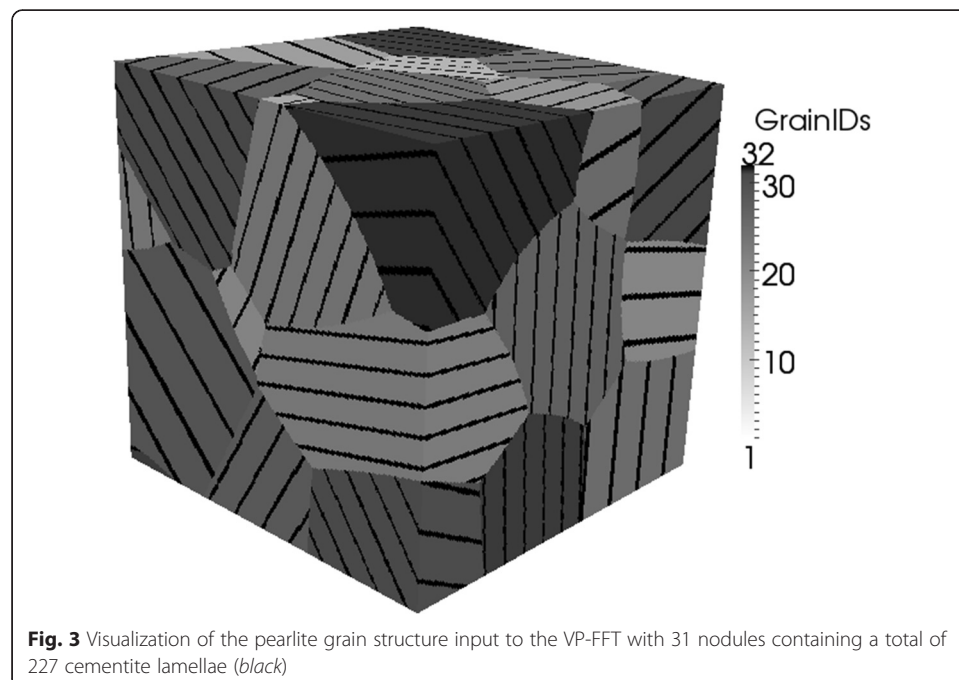


**Fig. 3** Visualization of the pearlite grain structure input to the VP-FFT with 31 nodules containing a total of 227 cementite lamellae (black)



## Results and discussion

### Copper

The 99.9999 % pure copper sample used in the HEDM study was selected because there is only one type of slip with no competing deformation mechanisms. Copper is a face-centered cubic (FCC) material with a slip on the close-packed  $\{111\}$  planes with  $\langle 110 \rangle$  Burgers vector, totaling 12 possible slip systems. As there exists only one slip mode, optimization of constitutive law parameters is fully independent (i.e., all parameters are varied independently). The result of the VPSC parameter optimization is shown in Table 1.

A VP-FFT simulation of the  $64 \times 64 \times 64$  subset of the measured copper specimen was performed using these parameters. Minor discrepancies are present between the VP-FFT and experimental stress-strain curves at strains less than 10 %. At strains larger than 10 %, the VP-FFT flow stress is larger than the experimental data. Adjustments to  $\tau_1$  and  $\theta_1$  can better align the VP-FFT with the other two datasets.

The largest difference, 10.9 MPa (4.2 % error), observed between the two computational results occurs at the final strain step. However, up to 10 % strain the two curves match quite well with a mean difference of 1.1 MPa. Initially, the results vary by 4.7 MPa (4.7 %) but quickly converge. Overall, the discrepancy between the two simulations is 4.0 MPa, on average. However, if the VPSC and VP-FFT simulations were carried out past 20 %, the curves would continue to diverge, increasing the mean discrepancy between curves.

Because VPSC operates on a per-grain basis, the mosaic spread in grain orientation as a result of plastic deformation, which has been observed during HEDM and electron backscattered diffraction (EBSD) [42–44], is not captured. Thus, the texture evolution of VPSC is expected to be an overestimate, while the local nature of VP-FFT has been shown previously to provide a more reasonable texture evolution, i.e., less rapid sharpening [3]. This may explain the deviations at high strains while maintaining good agreement at low strain.

Fine-tuning of the VP-FFT Voce parameters was not performed in the same MATLAB framework coupled with VPSC. With experience and understanding of the Voce hardening law, informed guesses at new parameters were made to bring the VP-FFT curve in line with the VPSC and experimental curves. To improve the fit at high strains, the  $\tau_1$  and  $\theta_1$  Voce parameters are adjusted by +1.4 and  $-10.4$  MPa, respectively. These specific changes were selected such that  $\tau_1$  and  $\theta_1$  were whole numbers, 17.0 and 75.0, respectively. By moving the back-extrapolated intercept higher (i.e., an increased  $\tau_1$ ) and decreasing the steady-state hardening rate (i.e., lowered  $\theta_1$ ), the small-strain data remain in good agreement while increasing agreement at higher strains. Comparison of the original fit and adjusted parameter stress-strain curves is

**Table 1** Best-fit VPSC and subsequent VP-FFT constitutive law parameters for FCC copper

	VPSC	VP-FFT
$\tau_0$ (MPa)	35.8	35.8
$\tau_1$ (MPa)	15.6	17.0
$\theta_0$ (MPa)	321.6	321.6
$\theta_1$ (MPa)	85.4	75.0



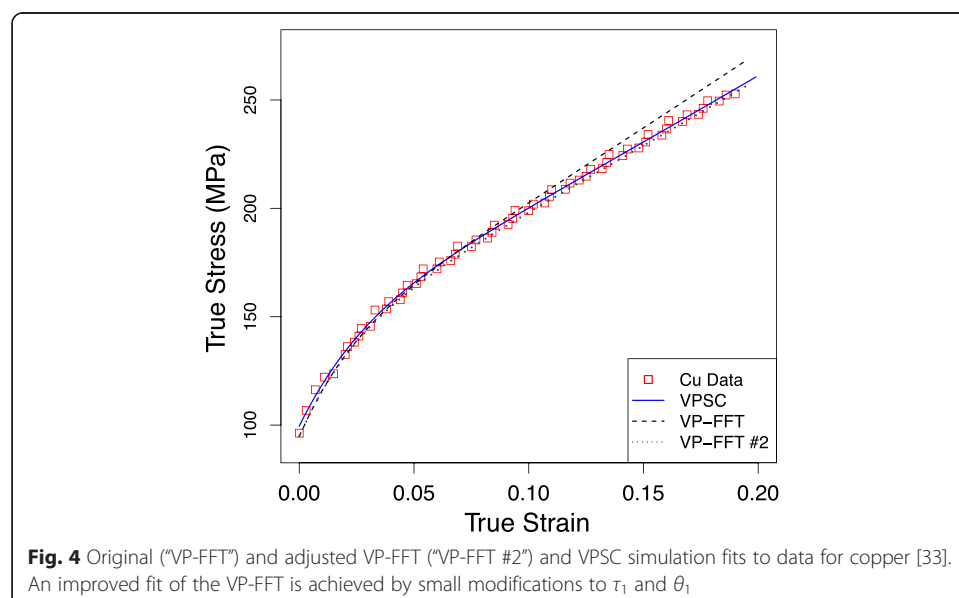
presented in Fig. 4. A more satisfactory fit is found between the two simulations. An average difference of 1.3 MPa over the 20 % strain range and only a 1.0-MPa (0.4 %) difference at the final strain are observed. Clearly, the adjusted parameters result in a VP-FFT result that matches the VPSC result well and, in turn, the experimental copper data. Changes in the  $\tau_1$  and  $\theta_1$  Voce parameters did not result in noticeable changes in crystallographic texture.

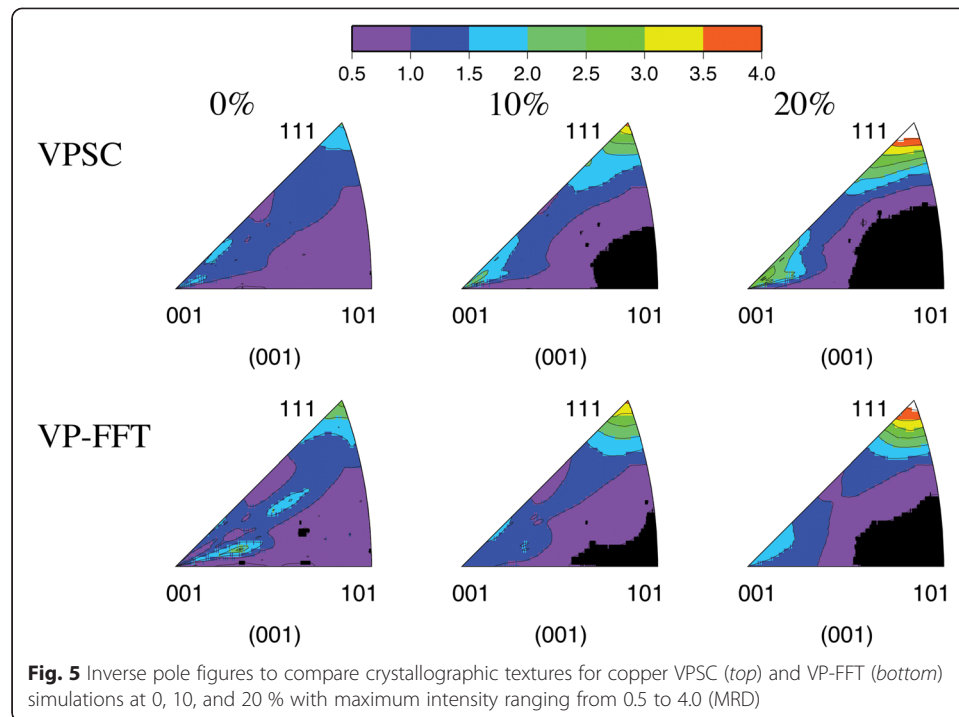
Development of crystallographic texture occurs as grains slip and rotate. Textures at 0, 10, and 20 % are presented in Fig. 5 for both VPSC and VP-FFT. Minor differences in multiples of a random distribution (MRD) of the starting texture occur, where a random texture has an MRD = 1.0, with VPSC having a lower MRD (1.5) than VP-FFT (2.5) in the  $\langle 111 \rangle$  corner. Further deformation strengthens this texture ( $>4$  MRD). At 10 % strain, VPSC and VP-FFT have similar textures (3.5 MRD). At 20 % strain, VPSC and VP-FFT have an MRD  $> 4$ . However, the VPSC 4 MRD contour is larger, indicating that the peak in MRD is higher. Thus, VPSC starts at a more random texture and ends with a sharper texture. Therefore, VPSC rotates orientations at a higher rate than VP-FFT (i.e., over-predicting crystallographic textures).

#### IF steel

A body-centered cubic steel provides two slip modes with relatively similar potential for a slip. These slip modes are  $\langle 111 \rangle$  Burgers directions with  $\{110\}$  slip planes and  $\langle 111 \rangle$  Burgers directions with  $\{112\}$  slip planes. It was assumed that the hardening behavior of these slip modes was captured by the same set of parameters to reduce optimization complexity. This optimization required approximately 1 h to complete on a standard work station. The parameters are given in Table 2.

A VP-FFT simulation of the  $256 \times 256 \times 256$  IF steel microstructure with random orientations was performed using this set of parameters. The VP-FFT stress-strain response is shown in Fig. 6 along with VPSC and experimental data. The degree of agreement between VPSC and experimental data is quite high. Coincidence of VP-FFT





and VPSC data is high at small strains with increasing divergence at higher strains. As discussed in the previous section, adjusting the  $\tau_1$  and  $\theta_1$  parameters is required for a better fit. They are decreased by approximately 2 and 4 MPa, respectively. Upon adjustment, the curves then coincide up to 20 % strain. The adjusted VP-FFT response is also plotted in Fig. 6.

To compare computation times, VPSC and VP-FFT IF steel simulations were run with 100, 200, and 400 grains on VP-FFT domains of size  $32^3$ ,  $64^3$ , and  $128^3$  material points. Details of the total strain and strain steps are the same as those used above. VPSC simulations are executed on a personal laptop with a 2.9-GHz Core i7 processor, while VP-FFT simulations are executed on the DoD ERDC Supercomputer *Garnet* with 32 2.5-GHz AMD Interlagos Opteron processors per simulation. On average, each VP-FFT strain step required 57 iterations to reach an equilibrated solution. Computation times for these simulations are listed in Table 3. VP-FFT computation times are the total amount of time used on all processors. VPSC's speed advantage is clear from these computation times for comparable simulations. Additionally, it is clear that VPSC computation times depend solely on the number of grains in the simulation, while VP-FFT computation times depend solely on domain size. This indicates that the majority of the computational effort is associated with solving the non-linear equation for the stress state, Eq. (2), at each point or grain regardless of how the interaction between each point or grain and the surrounding medium is handled, i.e., the FFT is a minor part of the cost.

### Pearlite

The philosophy of the approach used for obtaining the Voce hardening parameters for pearlite is to first decompose an experimental plastic stress-strain curve of pearlite into

**Table 2** IF steel VPSC optimized and subsequent VP-FFT Voce hardening parameters

	VPSC	VP-FFT
$\tau_0$ (MPa)	54.3	54.3
$\tau_1$ (MPa)	42.2	40.0
$\theta_0$ (MPa)	619.2	619.2
$\theta_1$ (MPa)	106.8	103.0

separate curves for the response of pearlite and cementite using measurements of stress segregation upon loading. This is necessary due to the brittle nature of cementite in the absence of a lamellar structure. Optimization is performed on the single-phase curves individually with a composite VPSC simulation performed as a check of the optimization. While VP-FFT accounts for the grain structure and subsequent cementite lamellar network, VPSC can only do this in a limited fashion [45]. Therefore, corrections must be made to  $\tau_0$  for both phases due to the lamellar structure. Corrections for ferrite are made with a size scale argument while corrections of cementite are made via a guess-and-check method within the VP-FFT.

Pearlite has a lamellar structure of ferrite and cementite with spacing on the order of a micrometer. Clearly, this is a complicated nano-composite, and the physics that describe the deformation of each constituent phase [46–49] suggests that more sophisticated models could be used, especially for cementite. Nevertheless, for the VPSC and VP-FFT methods that employ the extended Voce model (Eq. 3) to describe the stress-strain response, the approach developed in this manuscript offers an efficient approach to develop a constitutive relation for this class of material. Where more detailed data is available, such as multiple different strain paths, more complex models, e.g., latent hardening, may be justified.

Pearlitic ferrite is crystallographically similar to the IF steel studied above and deforms via the same slip systems. Cementite’s six primary slip modes are comprised of [001], [010], and [100] slip directions and (001), (010), and (100) slip planes. These are unique and should ideally be treated as such; however, the hardening parameters for

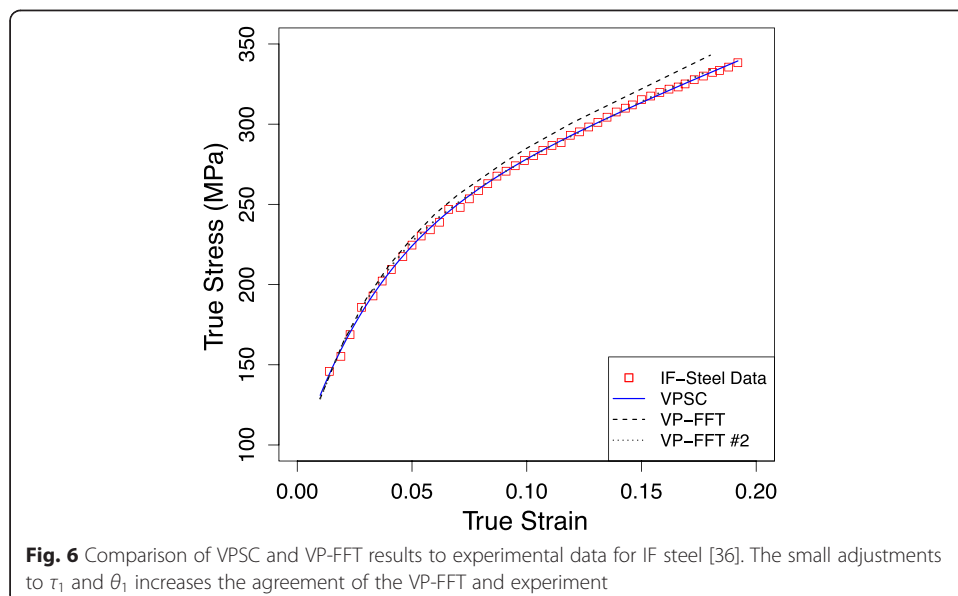


**Table 3** Computational time required for various size models. VPSC is performed on a standard personal laptop 2.9-GHz Core i7 processor, and VP-FFT is performed on the DoD ERDC Supercomputer "Garnet" with 32 2.5-GHz AMD Interlagos Opteron processors per simulation

# grains	Resolution	VPSC (s)	VP-FFT (min)
100	32 <sup>3</sup>	8	23.7
	64 <sup>3</sup>	8	91.7
	128 <sup>3</sup>	8	636.1
200	32 <sup>3</sup>	14	22.0
	64 <sup>3</sup>	14	90.2
	128 <sup>3</sup>	14	622.3
400	32 <sup>3</sup>	26	22.0
	64 <sup>3</sup>	26	90.2
	128 <sup>3</sup>	26	628.2

these six slip systems are assumed to be identical for computational tractability. This assumption is also applied to the six  $\langle 100 \rangle \{110\}$ <sup>1</sup> and the 12  $\langle 111 \rangle \{110\}$  slip modes separately. If only the cube slip systems are included, then only three independent directions are possible (i.e., [001], [010], and [100]) and arbitrary deformation would not be possible, i.e., a von Mises criterion is not satisfied. Therefore, the inclusion of the  $\langle 100 \rangle \{110\}$  and  $\langle 111 \rangle \{110\}$  cementite slip modes is necessary to ensure five independent slip systems are available for slip for an arbitrary deformation. The authors know no experimental evidence that quantifiable amounts of slip occur on these modes [50–53]. To provide five independent slip systems while minimizing the slip activity on the  $\langle 100 \rangle \{011\}$  and  $\langle 111 \rangle \{110\}$  slip modes,  $\tau_0$  for these modes is scaled by a factor  $\beta$ , which is the average ratio of the Burgers vector magnitude and interplanar spacing,  $b/d$ , for all slip systems [50] within the slip mode compared to that of  $\langle 100 \rangle \{001\}$  (i.e.,  $\beta$  for  $\langle 100 \rangle \{001\} = 1.00$ ). The  $b/d$  ratio is a measure of a system's barrier to slip. An ideal slip system has a large interplanar spacing and a small Burgers vector. Hence,  $b/d$  will be small. Therefore, the  $\tau_0$  for  $\langle 100 \rangle \{001\}$  can be specified, and  $\tau_0$  for the other slip modes is calculated.  $\beta$  values for  $\langle 100 \rangle \{011\}$  and  $\langle 111 \rangle \{110\}$  are 2.092 and 3.809, respectively.

The curve used for fitting pearlite parameters exhibits a similar behavior at low strains to the response of the IF steel curve. However, owing to the small strains tested for the IF steel, the large-strain Voce parameters (i.e.,  $\tau_1$  and  $\theta_1$ ) cannot be considered to be reliable for use in pearlitic ferrite. Therefore, a new comparison curve is selected for the large strains tested.

Cementite's high strength and network of interconnected lamellae in the fully pearlitic microstructure will require a higher stress to achieve the prescribed overall deformation. Therefore, cementite is expected to be the limiting phase in pearlite. The apparent yield stress of cementite is  $\sim 1500$  MPa [54] while the generally accepted yield stress of pearlitic ferrite without length effects is 70 MPa. Therefore, it is reasonable to expect yield stress values in cementite to be on the order of ten times larger than ferrite.

Assumptions are required to decompose the single curve into individual contributions. Tomographic measurements of pearlite have shown that ferrite controls the low-strain hardening behavior while cementite controls large-strain hardening behavior [36, 54].

Therefore, the ferrite curve used for comparison is those pearlite values below 35 % strain and the linear extrapolation of data above 35 % strain. The cementite curve is the linear back-extrapolated data before 35 % strain. To account for the enhanced hardening relative to ferrite, the curve used for comparison above 35 % strain is the sum of the pearlite data and the difference of the pearlite data and linear extrapolation above 35 % strain (i.e., those values used for ferrite above 35 %), up to 70 %. A depiction of the stress-strain curve deconstruction is shown in Fig. 7. The resultant hardening parameters from the VPSC optimization are listed in Table 4 with the resulting VPSC stress-strain curves shown in Fig. 8. An excellent fit of the VPSC composite and pearlite data is observed save for a small translation.

While VPSC is an efficient tool for finding Voce hardening parameters, it cannot account for the load transfer that takes place in the lamellar cementite structure; thus, overestimating  $\tau_0$  for ferrite by a factor of 2 and underestimating it for cementite by a factor of 10 for the final parameters are discussed below and listed in Table 4. This is the same factor by which the yield stress varies between pearlitic ferrite and cementite. That is to say that this is evidence that VPSC (and thus the optimization) fails to account for the structural network found in real pearlite microstructures. Therefore, these values must be adjusted within the VP-FFT or set by theory. Changes to  $\tau_0$  of either phase do not change the hardening behavior except to translate the curve up or down in stress.

The deformation behavior of pearlite is highly dependent on the microstructural characteristics. In particular, the yield stress is strongly correlated to the interlamellar spacing. Typically, an inverse or inverse-square root dependence is observed. The influence of the interlamellar spacing of cementite on pearlite used here is

$$\sigma_y = kS_0^{-1} + \sigma_\infty, \tag{4}$$

where  $\sigma_y$  is the yield stress,  $k$  the slope,  $S_0$  the interlamellar spacing, and  $\sigma_\infty$  is the yield stress of an infinite diameter grain. Because it is assumed that ferrite controls the

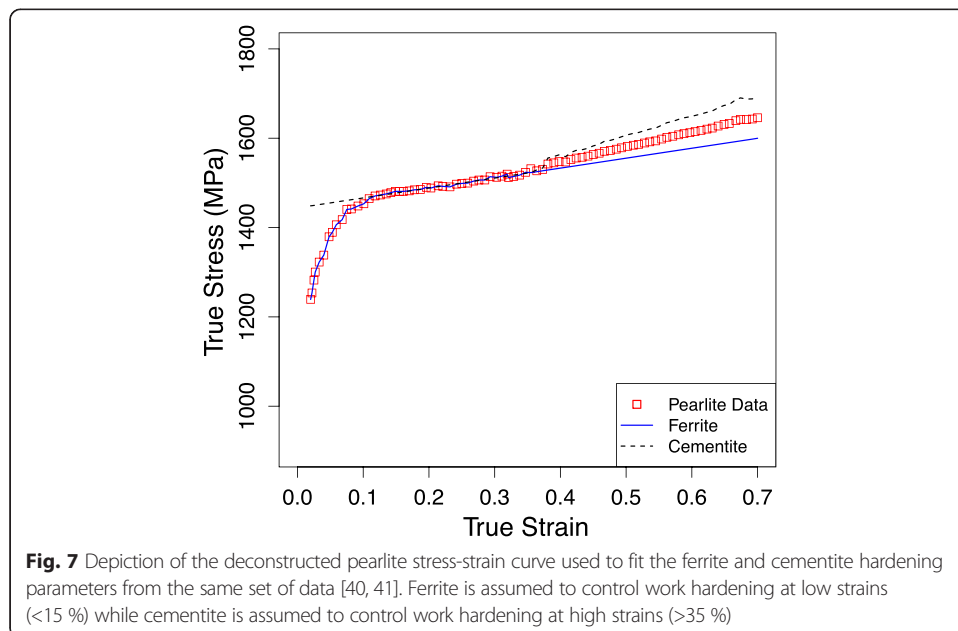


**Table 4** List of Voce constitutive law parameters (MPa) for pearlite

	Original $\tau_0$ (MPa)	Final $\tau_0$ (MPa)	$\tau_1$ (MPa)	$\theta_0$ (MPa)	$\theta_1$ (MPa)
Ferrite <111> {110}	444.3	185.8	170.6	2027.9	11.0
Ferrite <111> {112}	444.3	185.8	170.6	2027.9	11.0
Cementite <100> {001}	322.2	2726.0	1.215	0.276	628.9
Cementite <100> {011}	674.1	5702.1	1.215	0.276	628.9
Cementite <111> {110}	1227.4	10383	1.215	0.276	628.9

deformation at low strains, this relationship is applicable in ferrite only. The slope,  $k$ , is 50 MPa/ $\mu\text{m}$  [55, 56] given in the macroscopic scale yield stress. As mentioned previously, to bridge the disparate macro- and meso-scales, a Taylor factor,  $M$ , is used. Here, we use the average Taylor factor in the IF steel VP-FFT calculation (2.376). The IF steel optimized  $\tau_0$  is used as the  $\sigma_\infty$  in this relationship as it is compositionally similar to pearlitic ferrite.

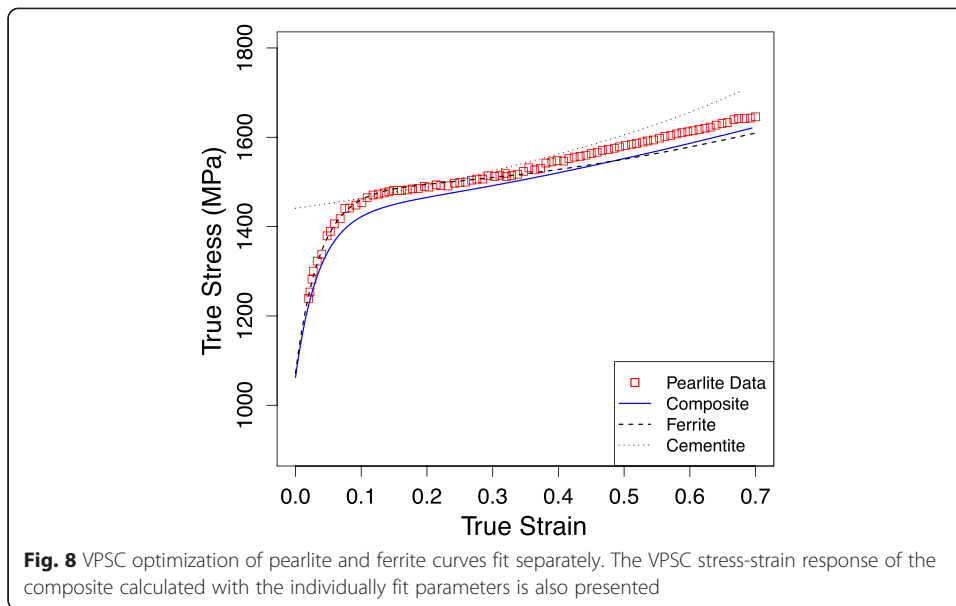
$$\text{CRSS} = \frac{\sigma_y}{M} = \frac{kS_0^{-1} + \sigma_\infty}{M} = \frac{kS_0^{-1}}{M} + \tau_0^{\text{IF steel}} \quad (5)$$

The computed  $\tau_0$  for ferrite, 185.8 MPa, with a 0.16- $\mu\text{m}$  interlamellar spacing is used in the VP-FFT simulation.

Note that, although the compositions of IF steel and pearlitic ferrite are similar, their hardening mechanisms may differ (i.e., precipitation hardening versus solid solution strengthening). Nano-indentation is a possible alternative method for estimating  $\tau_0$  for pearlitic ferrite. However, the IF steel test data available in the literature was convenient for the estimates required for the method developed in this manuscript. Additionally, this inaccuracy in this portion of the pearlite model is likely minimal considering the much larger  $\tau_0$  for cementite.

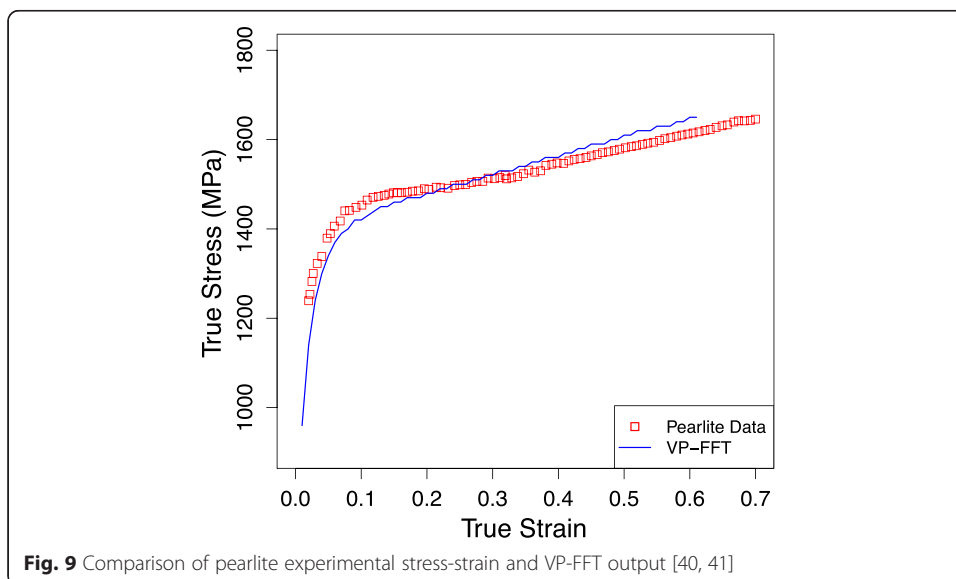
Due to the inability of VPSC to take into account the lamellar structure of pearlite, adjustments to cementite  $\tau_0$  were performed via trial-and-error VP-FFT simulations.  $\tau_0$  for the cementite <010> {001} slip mode was found through VP-FFT adjustments with an initial guess coming from VPSC. Initial CRSS values for the other slip modes are determined by the  $\beta$  parameter described previously. Despite the polycrystalline cementite and ferrite structures used in VPSC optimization, the remaining Voce hardening parameters,  $\tau_1$ ,  $\theta_0$ , and  $\theta_1$ , were constant for all slip modes of ferrite and cementite. Table 4 lists the Voce hardening parameters used for all phases and slip modes in all subsequent VP-FFT calculations. These hardening values show the control of the initial hardening rate by ferrite (i.e., small  $\theta_0$  for cementite) and the final hardening rate by cementite (i.e., small  $\theta_1$  for ferrite).

Figure 9 shows a comparison of the experimental data and the VP-FFT output. While the initial difference between responses is sizeable, 99.2 MPa (8.0 %), an effort was made to maximize overall agreement, by visual inspection after each VP-FFT simulation of the candidate  $\tau_0$  cementite parameters. In particular, focus was placed on the strain range 15–30 % where the final average absolute difference is 8.6 MPa. Visually, the VP-FFT response beyond 25 % strain hardens at a faster rate than the physical experiment as evidenced by the nearly identical stresses at 25 % and the larger VP-FFT stress by 32.5 MPa (2.0 %) at the maximum simulated strain. While these differences are noticeable, no further adjustments to  $\tau_1$  and  $\theta_1$  are made because the discrepancies between



simulation and experiment can no longer be attributed to a single phase. Manual adjustments would nullify the computational advantages obtained by employing the MATLAB/VPSC optimization and may disregard the assumptions made in the development of this pearlite constitutive law.

In comparison to Cu and IF steel, the fit to pearlite is less accurate. This may be attributed to numerous factors including the development of dislocation structures within the ferrite that control the ferrite deformation at progressively higher strains [46–49]. The VPSC and VP-FFT methods and the simple Voce hardening model (Eq. 3) do not sufficiently account for the physics of such phenomena. Additionally, there exist collinear slip directions at the ferrite-cementite interface in the Bagaryatsky orientation relationship (i.e.,  $[010] \text{Fe}_3\text{C}$  parallel to  $[111] \text{Fe}$ ) that can account for additional hardening. However, this effect of latent hardening is not accounted for in the





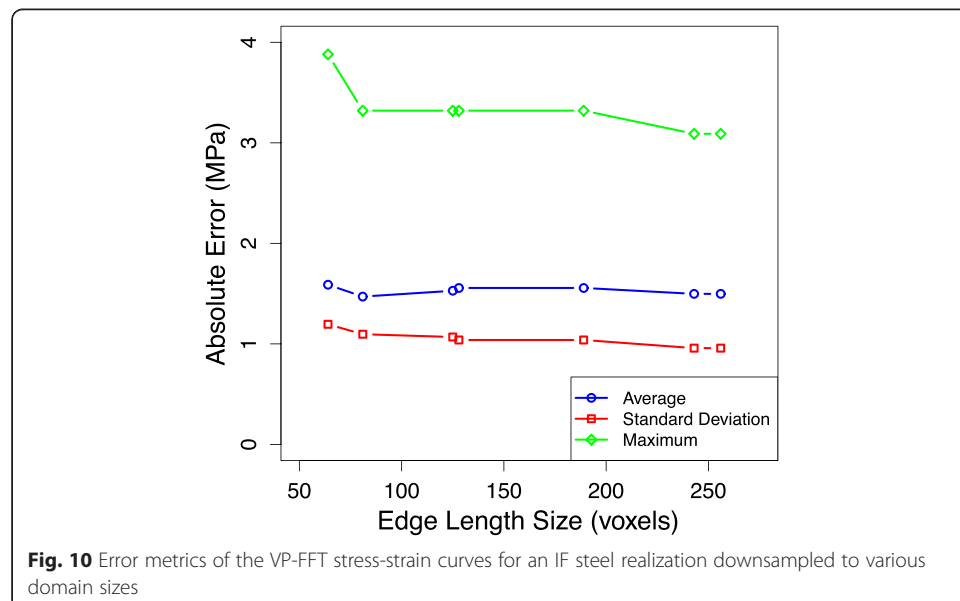
Voce hardening model employed here. This leads to the difficulties observed in providing the excellent match between the test data and simulation responses observed in Cu and IF steel. This final case study may extend beyond the intended capabilities of the VPSC and VP-FFT methods, but the approach described in this manuscript still is useful for reducing the time required to obtain model parameters to describe the compatible deformation of a lamellar structure of ferrite and cementite.

**Domain size dependence**

It has been reported that the Voce parameters required to achieve a given stress-strain response are dependent on the domain resolution [57]. VP-FFT simulations were repeated for IF steel microstructures downsampled to cubic domains with edge lengths 64, 81, 125, 128, 189, and 243 voxels from the domain with edge length 256 voxels. Only a single grain with original volume of 65 voxels was removed during downsampling in the domain with edge length 189 and smaller. Absolute differences between each VP-FFT and experimental responses are computed at matching strain levels only (i.e., intermediate strain experimental data points are ignored in comparisons) because simulations use a strain step of 1 %. This comparison is shown in Fig. 10.

While higher resolutions afford more degrees of freedom and higher potential for mosaic spread of crystal orientations, the viscoplastic constitutive response of the crystal is largely independent of domain resolution. For example, in the previous section the large difference in VPSC and VP-FFT model resolutions results in a very small difference in stress-strain response with equivalent Voce parameters. This is confirmed as no domain response varied by more than 2.0 MPa on average, with a maximum deviation of 3.88 MPa at 6 % strain at the lowest domain resolution. It is clear from this analysis that no dependence on domain size is present for simply polycrystalline microstructures within VP-FFT.

Note that while this work has focused on fitting the predicted stress-strain behavior, both codes also simulate texture evolution. Thus, one could utilize an optimization that



tracks both stress-strain and texture, which would require two limit states as opposed to one. This would require a different optimization algorithm, but there are no obvious obstacles to implementation.

## Conclusions

There is a significant difference in computational time required between the VPSC and VP-FFT codes, Table 3. Thus, this study provides a method for reducing the amount of time required to fit experimental stress-strain data with the VP-FFT code. Applying the Voce parameters optimized through the VPSC to the VP-FFT code saves the user time and removes guesswork from the fitting process.

The utilization has been illustrated through a viscoplastic self-consistent model [2] for rapid fitting of the Voce model to experimental stress-strain data through use of MATLAB's built-in optimization toolbox. The optimized parameters were shown to be valid in the computationally time-consuming but higher fidelity VP-FFT code. For high-purity copper, the parameter values derived with VPSC were immediately usable in the VP-FFT code and only the initial CRSS value required adjustment.

Applying this method to a pearlitic, biphasic steel resulted in a drastic decrease in the amount of time required to develop an acceptable hardening model for the VP-FFT code by decreasing the number of high-resolution simulations required. The parameters derived from VPSC provided a well-informed initial guess that required minimal change in order to properly fit the experimental stress-strain curve. This demonstrated that the method is not limited to a single-phase material. With sufficient knowledge of each individual phase, a two-phase material constitutive law can be developed.

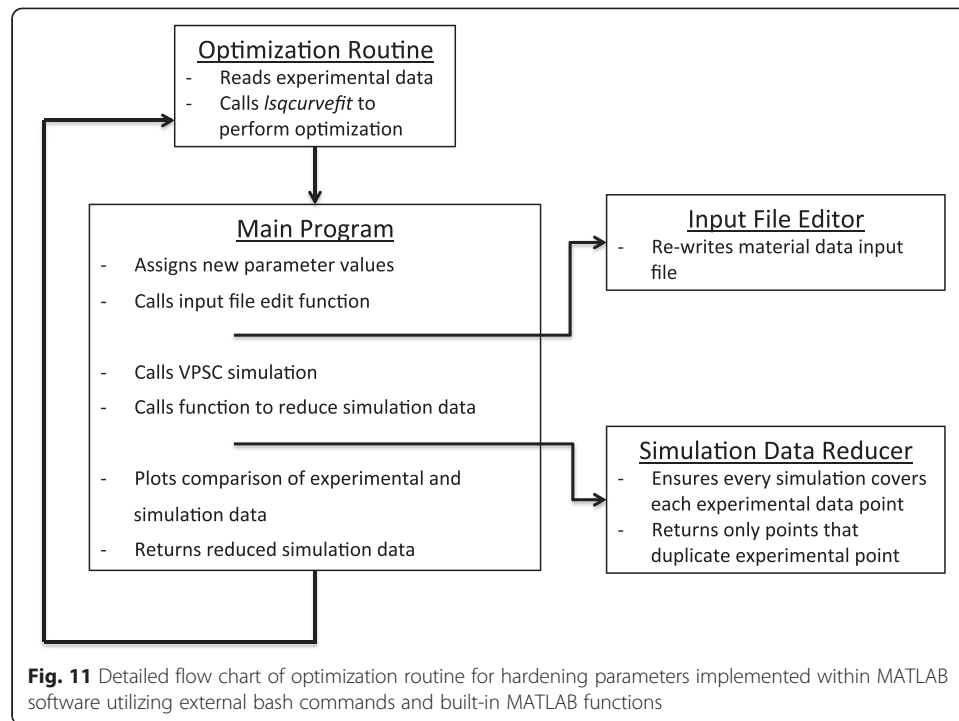
## Endnotes

<sup>1</sup>The notation for families of crystallographic planes and directions is extended here to include the set of slip planes and directions with permutations of the indices that are distinguishable within the orthorhombic cementite crystal.

## Appendix I: details of MATLAB optimization routine

The optimization routine used to develop the Voce hardening parameters throughout this paper was written in MATLAB 2012 using the *lsqcurvefit* function built into the Optimization toolbox. The *lsqcurvefit* function uses a non-linear, least-squares optimization technique that seeks to minimize the sum of the square of the residuals. Because the problem is inherently non-linear, an iterative approach is used. MATLAB's ability to call externally compiled programs was exploited for this work, and a detailed flow chart can be seen in Fig. 11.

The optimization routine, as mentioned previously, utilized the *lsqcurvefit* function. However, the function requires data points against which it calculates the residual and performs the optimization. Once the data has been read in, the *lsqcurvefit* function calls the "main program" in order to generate the simulated data points. The main program starts by assigning the updated parameter values (as dictated by the least-squares algorithm). Once this has occurred, the input file editing function is called to write the new parameter values to the input file (external text file) and then return a success (or error) flag to the main program. The



externally compiled VPSC program is then called using the `!` command within MATLAB, which allows the calling of the external program. Once VPSC has completed the simulation, the output files (text files) are read back into MATLAB. The simulated stress-strain data is then passed, along with the experimental data, to the data reducing function. This function reduces the full-scale simulation data to a list of stress-strain points that coincide precisely with the experimental data provided. Thus, if there are 80 experimental data points, the reducing function will return exactly 80 simulated points. The reason behind this reduction is that the *lsqcurvefit* function requires simulated values to match each strain point without any extra information. Since experimental data does not come from a continuous function, the simulated data must be reduced to a finite number of matching points.

After the reducing function has passed the reduced data back to the main program, the program generates a plot to pictorially inform the user the state of the optimization. The main program then passes the simulated stress data back to the optimization program so that the *lsqcurvefit* function is able to calculate the residual and generate new parameters.

A limitation of the *lsqcurvefit* function is that it uses a single set of maximum and minimum values to control how large of changes can occur during the optimization. Because the Voce hardening parameters can be orders of magnitude different, the *lsqcurvefit* optimizes multipliers (starting a value equal to 1) instead of optimizing the parameter values directly. Thus, the maximum and minimums are set at 0 and 10, respectively, and the minimum change is  $1E-2$ . This allows enough fidelity for fine adjustments but does not allow the large magnitude of  $\theta$  to overshadow the  $\tau$  values.

**Competing interests**

The authors declare that they have no competing interests.

**Authors' contributions**

BSA performed all the work related to the VP-FFT simulations. BTG integrated VPSC with MATLAB's optimization toolbox and performed the VPSC optimization of constitutive law parameters. BSA and BTG contributed equally to this manuscript with focus on the VP-FFT and optimization/VPSC sections, respectively. ADR provided oversight for the entirety of this work and provided editorial comments of this manuscript. All authors read and approved the final manuscript.

**Acknowledgements**

Use of the *Garnet* machine at the ERDC DSRC for completion of this work is gratefully acknowledged. The support of the High Performance Computing Modernization Office via the Productivity Enhancement, Technology Transfer and Training (PETTT) program is also acknowledged.

**Funding**

This research was supported in part (BSA) by an appointment to the Postgraduate Research Participation Program at the U.S. Army Research Laboratory administered by the Oak Ridge Institute for Science and Education through an interagency agreement between the U.S. Department of Energy and USARL. ADR acknowledges support from the National Science Foundation under DMR 1435544.

**Author details**

<sup>1</sup>Materials Response and Design Branch, US Army Research Laboratory, 4600 Deer Creek Loop, Aberdeen Proving Ground, MD 21005, USA. <sup>2</sup>U.S. Air Force Research Laboratory, Wright-Patterson, OH 45433-7817, USA. <sup>3</sup>Department of Materials Science and Engineering, Carnegie Mellon University, 5000 Forbes Ave, Pittsburgh, PA 15213, USA.

Received: 7 April 2016 Accepted: 18 May 2016

Published online: 19 July 2016

**References**

- Chaboche JL (2008) *Int J Plast* 24:1642–1693
- Lebensohn RA, Tome CN (1993) *Acta Metall* 41:2611–2624
- Lebensohn RA (2001) *Acta Mater* 49:2723–2737
- Rollett AD, Rohrer GS, Suter RM (2015) *MRS Bull* 40(11):951–960
- Abdul-Hameed H, Messager T, Zairi F and Nait-Abdelaziz M (2014). In: Rodrigues H, Herskovits J, Soares C.M, Guedes J.M, Araujo A, Folgado J, Moleiro F, and Madeira J.A (ed) *Engineering Optimization 2014*. Taylor & Francis Ltd., London, UK
- Zhang C, Moore JD (1997) *Polym Eng Sci* 32(2):414–420
- Shi S, Yu D, Gao L, Chen G, Chen J, Chen X (2012) *J Power Sources* 213:40–46
- Ran JO, Fu MW (2014) *Int J Plast* 61:1–16
- Wang H, Wu PD, Gharghoury MA (2010) *Mater Sci Eng, A* 527:3588–3594
- Wang H, Wu PD, Tome CN, Wang J (2012) *Mater Sci Eng, A* 555:93–98
- Staroselsky A, Anand L (2003) *Int J Plast* 19:1843–1864
- Balsubramanian S, Anand L (2012) *J Mech Phys Solids* 50:101–126
- Smith A, Chen Z, Lee JY, Lee MG, Wagoner RH (2014) *Int J Plast* 58:100–119
- Zhang K, Holmedal B, Hopperstad OS, Dumoulin S, Gawed J, Van Bael A, Van Houtte P (2015) *Int J Plast* 66:3–30
- Gonzalez D, Simonovski J, Withers PJ, Quinta Da Fonseca I (2014) *Int J Plast* 61:49–63
- Yang BJ, Shin H, Kim H, Lee HK (2014) *Appl Phys Lett* 104:1–4
- Ma LJ, Liu XY, Fang Q, Xu HF, Xia HM, Li EB, Yang SG, Li WP (2013) *Rock Mech Rock Eng* 46:53–66
- Sun L, Zhu Y (2013) *Construct Build Mater* 40:584–595
- Barnett RA, O'Donoghue PE, Leen SB (2013) *Int J Fatigue* 48:192–204
- Follansbee PS, Kocks UF (1988) *Acta Metall* 36:81–93
- Lebensohn RA, Tome CN (1997) *Acta Metall* 45:3687–3694
- Lebensohn RA, Tome CN (1994) *Mater Sci Eng, A* 175:71–82
- Hu L, Banovic S, Foecke T, Iadicola M and Rollett AD (2009) *Proc. IDDRG 2009 International Conference, The International Deep Drawing Research Group*, pp. 285–294; <http://www.iddrg.com>, accessed June 2016.
- Lebensohn RA, Casteñeda PP, Brenner R and Castelnau O (2011) *Computational Methods for Microstructure-Property Relationships*. Ghosh, Somnath, Dimiduk, Dennis, Springer US
- Eshelby JD (1957) *Proc R Soc Lond A Math Phys Sci* 241:376–396
- Eshelby JD (1959) *Proc R Soc Lond A Math Phys Sci* 252:561–569
- Tome CN and Lebensohn RA (2012) *Manual for Code Visco-Plastic Self-Consistent (VPSC)*. [public.lanl.gov/lebensohn/VPSC7c\\_manual.pdf](http://public.lanl.gov/lebensohn/VPSC7c_manual.pdf)
- Voce E (1955) *Metallurgia: Brit J Metals* 51(307):219–226
- Taylor GI (1938) *J Inst Met* 62:307–324
- Rollett AD, Smith PR, James MR (1998) *Mat Sci Eng A - Structural Materials Properties Microstructure and Processing* 257:77–86
- Frigo M, Johnson SG (2005) *Proc IEEE* 93:216–231
- Anglin BS, Rollett AD, Lebensohn RA (2014) *Comput Mater Sci* 87:209–217
- Li SF, Lind J, Hefferan CM, Pokharel R, Liener U, Rollett AD, Suter RM (2012) *J App Crys* 45:1098–1108
- Pokharel R, Lind J, Li SF, Kenesei P, Lebensohn RA, Suter RM, Rollett AD (2015) *Int J Plast* 67:217–234
- Groeber MA, Jackson MA (2014) *Integrating Materials and Manufacturing Innovation* 3(5):1–17

36. Morooka S, Tomota Y, Kamiyama T (2008) *ISIJ Intl* 48:525–530
37. Inoue A, Ogura T, Masumoto T (1973) *J Jpn Inst Metals* 37(8):875–882
38. Ohashi T, Roslan L, Takahashi K, Shimokawa T, Tanaka M, Higashida K (2013) *Mater Sci Eng, A* 588:214–220.
39. Bagaryatsky YA, Dokl, Akad and Nauk (1950) *SSSR vol. 73*: pp. 1161–1164.
40. Sevilano JG, van Houtte P, Aernoudt E (1981) *Prog Mater Sci* 25:69–412
41. Sevilano JG (1974) PhD Thesis. Katholieke Universiteit, Leuven, Belgium, 1974
42. Jin HJ, Kurmanaeva L, Schmauch J, Rösner H, Ivanisenko Y, Weissmüller J (2009) *Acta Mater* 57(9):2665–2672
43. Hayashi Y, Hirose Y, Setoyama D (2014) *Mater Sci Forum* 777:118–123
44. Pokharel R, Lind J, Kanjarla AK, Lebensohn RA, Li SF, Kenesei P, Suter RM, Rollett AD (2014) *Rev Condens Matter Phys* 5 5:317–346
45. Lebensohn RA, Canova GR (1997) *Acta Mater* 45(9):3687–3694
46. Embury JD, Fisher RM (1966) *Acta Metall* 14:147–159
47. Langford G (1970) *Metall Trans A* 1:465–477
48. Langford G (1977) *Metall Trans A* 8A:861–875
49. Inoue A, Ogura T, Masumoto T (1977) *Metall Trans A* 8A:1689–1695
50. Sevilano JG (1975) *Mater Sci Eng* 21:221–225
51. Mauer K, Warrington DH (1967) *Philos Mag* 15(134):321–327
52. Inoue A, Ogura T, Masumoto T (1976) *Trans JIM* 17:663–672
53. Castelnau O, Blackman DK, Lebensohn RA and Castañeda PP (2008) *J Geophys Res: Sol Earth* vol. 113.
54. Tomota Y, Lukáš P, Neov D, Harjo S, Abe YR (2003) *Acta Mater* 31:805–817
55. Elwazri AM, Wanjara P, Yue S (2005) *Mater Sci Eng, A* 404:91–98
56. Marder AR, Bramfitt BL (1976) *Met Trans A* 7A:365–372
57. Pokharel R (2013) PhD. Thesis. Carnegie Mellon University, Pittsburgh, PA, USA

**Submit your manuscript to a SpringerOpen<sup>®</sup> journal and benefit from:**

- Convenient online submission
- Rigorous peer review
- Immediate publication on acceptance
- Open access: articles freely available online
- High visibility within the field
- Retaining the copyright to your article

---

Submit your next manuscript at ► [springeropen.com](http://springeropen.com)

---